Operando UV-Raman study of the methanol to olefins reaction over SAPO-34: Spatiotemporal evolution monitored by different reactor approaches

DOI:10.1016/j.cattod.2018.11.065

Operando UV-Raman study of the methanol to olefins reaction over SAPO-34: spatiotemporal evolution monitored by different reactor approaches

Matteo Signorile[1*], Daniel Rojo Gama[2,3], Francesca Bonino[1], Stian Svelle[2], Pablo Beato[3], Silvia Bordiga[1]

[1] Department of Chemistry, NIS and INSTM Reference Centre, Università di Torino, Via G. Quarello 15, I-10135 and Via P. Giuria 7, I-10125, Torino, Italy

[2] Center for Materials Science and Nanotechnology (SMN), Department of Chemistry, University of Oslo, 1033 Blindern, 0315 Oslo (Norway)

[3] Haldor Topsøe A/S, Haldor Topsøes Allé 1, 2800 Kongens Lyngby (Denmark)

[*] Corresponding author: Matteo Signorile, matteo.signorile@unito.it

Abstract

A molecular understanding of coke formation during the methanol to olefins (MTO) reaction is of great importance in order to adopt strategies that can improve the lifetime of the catalyst. UV-Raman has proven to be a valuable characterization tool, because of the favorable resonance conditions achieved towards key coke components, e.g. aromatic and olefinic compounds. Still, the applicability of UV-Raman in MTO is limited by the high risk of inducing sample damage under the exposure to the intense UV excitation laser. This drawback has been addressed by specific experimental setups, exploiting the concept of sample movement under the laser beam during the measurement, so that the laser-sample interaction is minimized by averaging over a wider sample surface. In this work, the impact of two different experimental setups, both relying on sample movement, are evaluated for the operando investigation of the MTO reaction over a SAPO-34. While in one case the whole catalytic bed is moved (fluidized bed), in the other case the sample is pressed into a pellet and rotated. Due to the peculiar spatial evolution of the reaction zone during MTO in a fixed-bed reactor, each method provides valuable information, but at very different spatiotemporal scales.

Keywords

Methanol-to-hydrocarbons; Raman; Operando; Zeolite; Deactivation

1 Introduction

The methanol to hydrocarbons (MTH) reaction represents an industrially applied alternative to crude oil based processes, enabling the production of light olefins (MTO), gasoline (MTG) or aromatics (MTA), from abundant and economically viable feedstocks (e.g. natural gas, biomass or coal) [1–3]. The sustainable advantages of these processes are however hampered by the relatively fast deactivation of the zeolite catalysts on which the process relies [4]. Deactivation occurs by blockage of the active sites in the microporous network of the catalyst, as a consequence of heavy hydrocarbons and extended carbon deposits, in a process usually referred to as coking [5–7]. A molecular level characterization of the hydrocarbons transformations occurring during deactivation, is essential for obtaining an understanding of coking mechanisms [8]. Another challenge for an accurate characterization of the deactivation phenomena is that instead of post-mortem, [7–9] ideally one would like to perform the analysis under reaction conditions, i.e. operando conditions [10,11,20,12–19]. To tackle both of the aforementioned challenges, Raman spectroscopy has a considerable potential, but the number of literature reports dealing with the investigation of deactivation during MTH is still limited in comparison to other tools [10–13,21]. The advantages of Raman spectroscopy mostly relate to its capability in distinguishing among the several allotropic forms of carbon [22,23]. Furthermore, when wavelengths falling in the vicinity of the electronic transition of particular moieties are exploited, resonance conditions can be achieved for these ones. As a consequence, the intensities of some of the vibrational modes associated to these molecules are selectively enhanced by a factor 10^5-10^7 [24–26]. However, experiments performed with conventional visible laser sources often fail because of the strong overlap of the Raman signal with the fluorescence emission proper of aromatic species formed during MTH. Such interference is effectively avoided through a careful choice of the excitation wavelength, which should fall in a spectral range free from emission processes. UV excitation is a very convenient option, since the resonance conditions for some deactivation species are achieved: in particular, polycyclic aromatic hydrocarbons (PAHs) and other aromatic/conjugated species show their electronic transition in the mid-UV range, thereby allowing the resonance enhancement [27–29].

Besides the above mentioned multiple advantages, the application of UV-Raman spectroscopy in the MTH reaction has been mainly limited because of possible sample damaging under the intense UV irradiation. Therefore, the few authors that have applied UV-Raman spectroscopy to study the MTH reaction, also presented technical solutions able to overcome the sample damaging issue. The general concept beyond the experimental setups is sample movement: by continuously changing the portion of specimen exposed to the laser beam during the measurement, the spurious degradation induced by the excitation source is mitigated. In this way, a catalyst performing MTH can be monitored for a reasonably long time-framework, still obtaining trustworthy data. Several devices have been presented in the literature, mostly taking advantage of a mechanical movement of the sample (i.e. by spinning it through an electric engine) [30–32]. At the beginning of 2000, Chua and Stair developed a fluid bed reactor specifically for the in-situ investigation of the MTH reaction [11,12]: their device takes advantage of the continuous movement of the catalysts particles under the laser beam obtained through electromagnetic shaking of the whole reactor. They showed the effectiveness of their setup by measuring the spectra of several hydrocarbons related to MTH (e.g. benzene and PAHs), which appear stable even after hours of exposure to the UV laser beam. More recently, Beato et al. developed a micro-reactor cell based on the commercial Linkam CCR1000 setup [10]. Again, this tool takes advantages of the catalytic bed fluidization to achieve the sample movement. With respect to the technical solution described previously, in this reactor fluidization is produced with a fully fluid-dynamical approach: a membrane pump connected to the outlet of the cell produces an oscillatory backpressure, which makes the catalyst powder moving in a volcano like fashion. Among the proposed test cases, this setup has been applied to the study of MTH over ZSM-5 and ZSM-22.

Aiming to overcome some of the limitation of the previous devices (mostly related to the instability of the focus over the sample upon fluidization), some of us recently developed a mechanical-based setup, where the movement is produced through a magnetic stirring [33,34]. The latter has been exploited in a carefully controlled study of some relevant molecular species taking part to the deactivation in MTH (i.e. PAHs) [35], as well as in the characterization of pristine [36] and fully deactivated MTH catalysts with different topologies [8].

From the previous paragraph, the only reason driving the choice of a specific setup seems to be the necessity to avoid decomposition during the measurement. Actually, the choice of a different configuration can affect the observed process: this fact is of particular relevance for MTH, since the deactivation process has a spatial pattern determined by the type of reactor adopted. In fix bed designs the deactivation proceeds following the direction of the flow, in a way pictorially described as a “burning cigar” [18,19,37,38]. Conversely, in fluidized bed reactors deactivation reasonably occurs homogeneously over the whole catalyst, due to the continuous exchange of the position of particles with respect to the flow direction [39].

In the next sections, the UV-Raman characterization of SAPO-34 under MTO reaction conditions is reported. SAPO-34 represents the most applied catalyst for the MTO reaction because of its peculiar topology (see Figure 1).

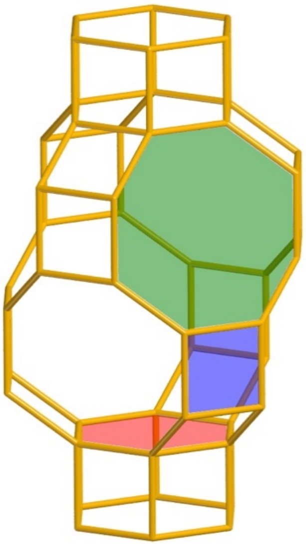

Figure 1. Topology (CHA) of SAPO-34. The main types of rings forming the framework are highlighted: 8-membered ring (green), 6-membered ring (red) and 4-memberd ring (blue).

The SAPO-34 framework belongs to the CHA topology: the network of double six rings includes quite large *cha* cages interconnected by small 8-membered ring windows. The latter allow the diffusion of molecules with dynamic radius smaller than 3.72 Å, whereas species up to 7.37 Å can be hosted in the cages [40]. Such features explain the superior selectivity of SAPO-34 toward light olefins (mostly ethylene and propylene) highly desirable in MTO, whereas bulkier hydrocarbons (including higher alkenes and aromatics) are trapped in the cages. The latter moieties, if not further able to react within the cages, become deactivating species which cause a progressive decrease of the catalysts activity down to complete deactivation. The aim of this work is to take advantage of the favorable resonance conditions achieved with UV-Raman towards key coke components and to characterize their formation/transformations under MTO conditions. Furthermore, the observed reactivity will be discussed on the basis of the specific reactor setup adopted for the measurement.

2 Materials and Methods

The SAPO-34 ((P+Al)/Si = 11) sample deeply characterized in ref. [8] have been studied under operando conditions in this work. UV-Raman spectra have been collected with a Renishaw inVia Raman Microscope spectrometer, whose excitation source is a Coherent MotoFred 300C frequency doubled Ar^+ laser, emitting at 244 nm. A 15× objective focused the excitation beam over the sample and recollected the backscattered light, then the Rayleigh peak was removed by a dialectic edge filter. The Raman signal was dispersed by a 3600 lines mm^{-1} grating and finally collected by a Peltier cooled CCD detector.

The operando UV-Raman measurements reported in this work have been performed taking advantage of two of the setups described in the Introduction section: the "magnetic stirring" and the modified Linkam CCR1000 setups. The key features of both setups are graphically outlined in Figure 2 and described thereafter.

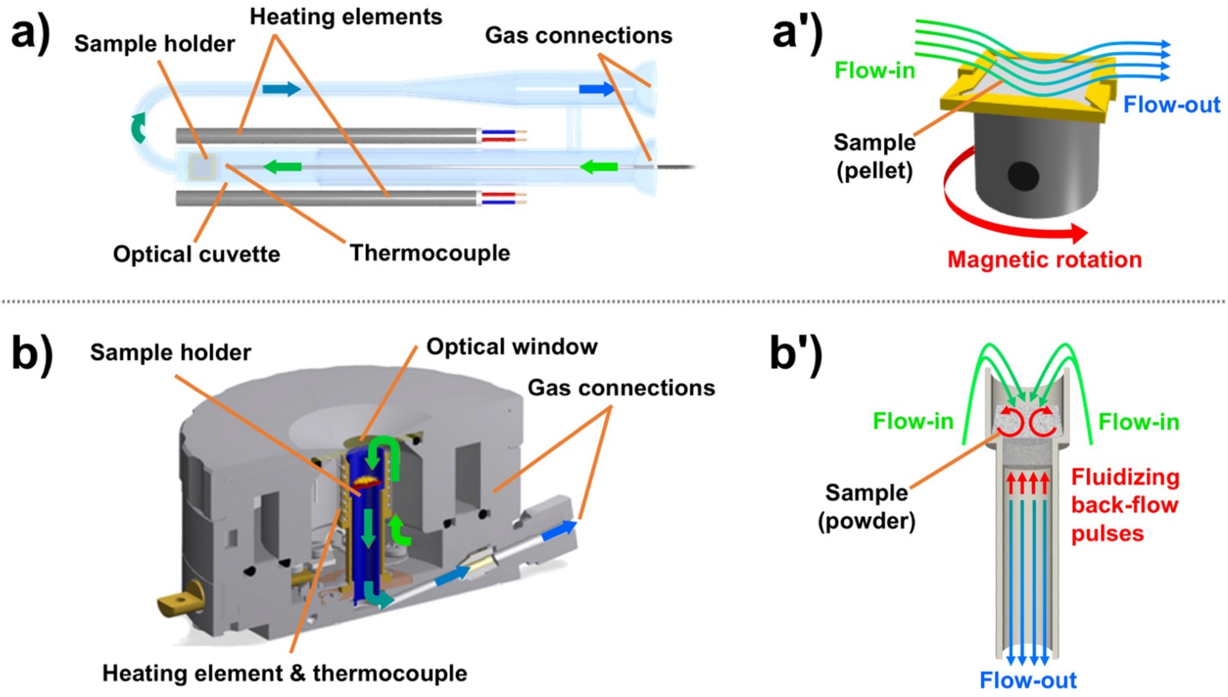

Figure 2. Schematics of a) magnetic stirring and b) modified CCR1000 setups. Panels a') and b') report details of the corresponding sample holders, highlighting the mechanism producing the sample movement during the measurements. Panel b) adapted from ref [10].

The magnetic stirring setup (Figure 2a) is derived from the house-made cell described in ref. [33,34] and is a simple U-shaped quartz-glass reactor, where a portion of the inlet channel is an optical grade quartz cuvette allowing the measurement of UV-Raman spectra. Furthermore, with respect to the parent cell, two external electrical heating elements are placed on the sides of the cuvette, allowing to span the 50-500 °C temperature range. The heating elements are controlled by a PID system driven by a K-type thermocouple, inserted in the cell nearby the sample and thus keeping constant the desired reaction temperature. The catalyst is mounted over a magnetic sample holder as a self-supported pellet of ~ 2 mg (Figure 2b): by applying an external magnetic field, the sample is put in rotation in order to perform reliable measurements. The gas flow crossing the cell tangentially hits the upper surface of the pellet, i.e. the same fraction of sample probed by UV-Raman. This measurement geometry can be thus regarded as a model for the top layers of a fixed bed catalyst.

The CCR1000 reactor is supplied by Linkam Scientific Instruments and it has been modified according to ref. [10]. In detail, the outlet of the reactor is connected to a membrane pump delivering back-flow pulses with a frequency of 40-100 Hz: the pressure fluctuations in the outgoing flow produces a fluidization of the catalytic bed, guaranteeing the reliability of the UV-Raman measurements. The catalyst (~ 20 mg) is loaded directly in powder form and measured under fluidized bed conditions, i.e. simulating a continuously stirred tank reactor (CSTR).

With both the setups, samples have been pre-oxidized at 550 °C under 20 ml min^{-1} of pure O_2 to remove the pre-existing carbonaceous residuals. After 30 min, the temperature has been decreased to 400 °C and, after purging with 20 ml min^{-1} of He for 5 min, the reaction has been started exposing the catalyst to methanol vapors (weight hourly space velocity, WHSV, of 2 g_{MeOH} g_{cat}^{-1} h^{-1}). In order to keep the WHSV to the desired value, the temperature of the methanol bubbler has been decreased to 0 °C in the case of the CCR1000 reactor and down to -20 °C for the magnetic stirring one. Since its onset, the reaction has been monitored for approximately 90 min of time on stream (TOS), with a continuous collection of spectra (~10 min accumulation each). The qualitative composition of the flow outgoing the reactors has been monitored with a Pfeiffer OmniStar GSD 320 O quadrupole mass spectrometer (MS) during the whole experiment. Ex situ measurements have been performed for the sake of comparison on the fully deactivated SAPO-34 as characterized in ref. [8]: the whole amount of catalyst recovered from the reactor has been milled prior the measurement, in order to obtain a spatially averaged picture of deactivating species.

3 Results and Discussion

3.1 Magnetic stirring reactor

The operando UV-Raman characterization of SAPO-34 during MTH within the magnetic stirring reactor cell is shown in Figure 3.

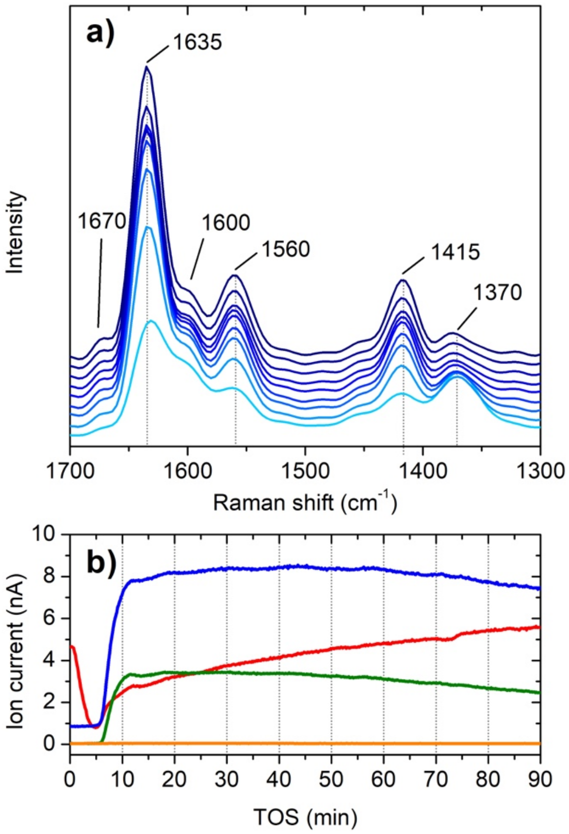

Figure 3. a) UV-Raman spectra of SAPO-34 along 90 min of MTH reaction (400 °C, 2 $g_{MeOH}\ g_{cat}^{-1}\ h^{-1}$) collected every 10 min (time evolution from cyan/bottom to blue/top) exploiting the magnetic stirring reactor cell. b) online MS charts for selected reagents/products: methanol (red, m/z = 31), ethylene (blue, m/z = 27), higher alkenes (green, m/z = 41) and aromatics (orange, m/z = 91).

Along the 90 min of reaction investigated in this study, a clear evolution of the spectroscopic features is observed. The maximum intensity variation is observed for the sharp peak with maximum at 1635 cm^{-1}, whose intensity rises by a factor 4 during the experiment and in particular during the first 30 min. The same band is actually red-shifted by approximately 5-10 cm^{-1} at the earliest stages. The bands at 1560 cm^{-1} and 1415 cm^{-1} grow simultaneously, with a similar intensity *versus* TOS trend. The two weak bands at approximately 1600 cm^{-1} and 1670 cm^{-1}, grow also with TOS but comparatively slower and to minor extent. The only band observed to decrease in intensity is the one at 1370 cm^{-1}, with a trend that seems to be directly inverse to the 1635 cm^{-1} band. Interestingly, the band at 1370 cm^{-1} also blue-shifts (~ 5 cm^{-1}) with increasing TOS.

Concerning the assignment of the observed UV-Raman signals, the concerted intensity trend suggests that the bands at 1635 cm^{-1}, 1560 cm^{-1} and 1415 cm^{-1} are related to the same or same group of chemical species. These can be related to alkenes [41]: this assignment is supported by the known retention of C_{4+} alkenes within the cages of SAPO-34, since the small 8-memeberd windows don't allow them to out-diffuse from framework [42]. The 1600 cm^{-1} is assigned to the G band of amorphous carbon, while the usually observed D band is suppressed due the use of UV excitation in its measurement [23]. The high frequency shoulder at ~ 1670 cm^{-1} falls in the region typical of carbonyl stretching, thus it can testify the presence of oxygenated compounds. However, some branched olefins can give signals up to this frequency value [41]. Finally, the 1370 cm^{-1} band is found in the frequency region typical of PAHs fingerprints [35]. Small PAHs give intense features close to this frequency, e.g. naphthalene (1380 cm^{-1}), anthracene (1400 cm^{-1}) and phenanthrene (1350 cm^{-1}), however none of them exactly match this band. It is important to highlight that the signal is rather broad (FWMH of ~40 cm^{-1}, i.e. roughly the double of ones of pure PAHs), indicating the overlap of the features of more than a single molecule. Furthermore, according to dissolution-extraction experiment performed on the same catalyst [8], these PAHs are most probably methylated and their skeletal vibration can be affected by such substitutions. The more abundant presence of PAHs at early TOS (according to the larger intensity of the 1370 cm^{-1} band) is further supported by the observed lower frequency of the most intense, band at about 1625 cm^{-1}: this frequency is characteristic for the small PAHs listed above.

The online MS signals reported in Figure 3b are a further piece of information useful in interpreting the chemical behavior of the catalyst during reaction. The most peculiar pattern is associated to methanol: at the beginning of the reaction, the ion current associated to it rapidly drops, while no products appear in the gas phase. As the signals from products start to appear, also the methanol signal starts to increase again, for a short time lapse with very high slope and then with a much slower rate until the end of the experiment. This peculiar evolution of the methanol signal is ascribed to the physisorption of methanol at the cold glass parts of the reactor cell and the concurrent build-up of the hydrocarbon pool in the pores of the zeolite. As all the glass parts are saturated by the methanol vapors, a higher fraction of it is able to pass through the whole reactor and is then measured by MS, causing the fast increase described above. On the other hand, the observed induction time before products are detected (typically between 5-10 min of TOS) has been discussed in the literature as a function of the primary size of the SAPO-34 particles [43]. At longer TOS, a progressive decrease in the catalysts activity is observed, according to the increase of the methanol signal and the simultaneous decrease of ethylene/propylene signals. Aromatics are never observed along the whole experiment, in agreement with the small-pore topology of CHA [8].

The combination of all the pieces of information above finally allows to describe the key hydrocarbons transformations occurring at the catalyst during the explored TOS. At early stages, when catalyst is still poorly productive, the dominating spectral features are ascribed to small, eventually methylated PAHs (the hydrocarbon pool) and a fraction of amorphous carbon (most probably sitting at the external surface of the catalyst particles). When products start to be observed by MS, the features of certain PAHs (1370 and 1625 cm^{-1}) decrease in intensity and signals related to alkenes (1635, 1560 and 1415 cm^{-1}) start to rise. The amount of bulk carbon slightly increases along TOS, as well as a low amount of carbonyl-containing species/branched alkenes is observed at late TOS. The observed MS and Raman signals evolution suggests that PAHs are part of the HCP under these reaction conditions: they are in fact observed with maximum abundance at the beginning of the reaction (while catalyst activity is increasing), then their amount decreases suggesting a transformation into other chemical species, probably larger PAHs (which are difficult to detect because of their decreased resonance with respect to smaller ones) [35]. The low increase of the bulk carbon features, further confirms that PAHs are converted into other molecular species rather than into extended coke. Instead, the growth and conservation of Raman signals related to long-chain and branched olefins, which are unable to diffuse out of the framework, indicate that they are not able to further react and consequently could act as deactivating-like species in SAPO-34. Such combination of aromatics and alkenes driving to deactivation in SAPO-34 is in line with the previous findings of Rojo-Gama et al.[8] and Hereijgers and co-workers [42].

3.2 *Linkam CCR1000 reactor*

The same operando experiment reported above has been repeated using a different reaction cell, i.e. the Linkam CCR1000, operated in a fluidized bed mode: the corresponding operando Raman spectroscopic and MS results are reported in Figure 4.

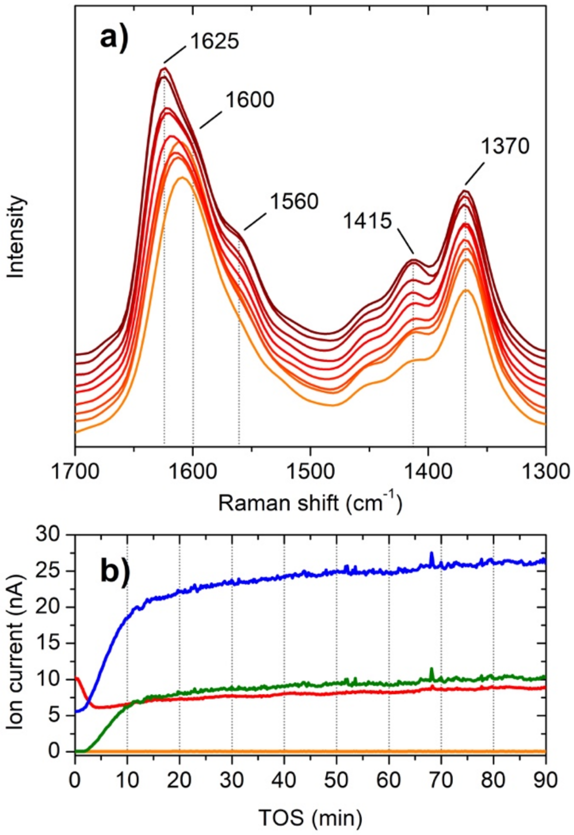

Figure 4. a) UV-Raman spectra of SAPO-34 along 90 min of MTH reaction (400 °C, 2 g_{MeOH} g_{cat}^{-1} h^{-1}) collected every 10 min (time evolution from orange/bottom to red/top) exploiting the Linkam CCR1000 reactor cell. b) online MS charts for selected reagents/products: methanol (red, m/z = 31), ethylene (blue, m/z = 27), higher alkenes (green, m/z = 41) and aromatics (orange, m/z = 91).

At a first look, the spectra reported in Figure 4a present similar spectral components as the ones previously discussed for Figure 3a. Nevertheless, their relative intensities are significantly different, with the exception of the first spectrum in the set reported in Figure 3a. At early TOS the dominating feature is the 1600 cm^{-1} component, which is however part of a broad band tailed toward higher frequencies. The only other clear band is located at 1370 cm^{-1}, and slightly increases in intensity with TOS. Concurrently, the maximum of the band at 1600 cm^{-1} is slowly masked with TOS by another band, significantly blue-shifted at a frequency of 1625 cm^{-1}. At the same time two weak bands at 1560 cm^{-1} and 1415 cm^{-1} increase in intensity.

It is reasonable to assign the bands to the same chemical species that where identified in the previous section for the magnetically stirred reactor. Accordingly, the band at 1600 cm^{-1} is related to amorphous carbon, the bands at 1370 and 1625 cm^{-1} to PAHs (probably methylated), and the two bands at 1560 and 1415 cm^{-1} to alkenes (including branched ones). The very intense peak of alkenes showed at long TOS in Figure 3a is not clearly visible in this set of data, however it is most probably present as inferred by the strongly asymmetric shape of the whole signal among 1500-1700 cm^{-1}, pronouncedly peaked toward the high frequencies.

The MS charts reported in Figure 4b appear smoother than in the previous experiment, with the methanol signal dropping with a knee-shape along the first 5 min and then stabilizing on a closely constant value. Both ethylene and propylene show onsets with the same trend but opposite sign, reaching the full productivity at ~ 10 min of TOS. Again, the delay among the methanol drop and the reaching of complete productivity are ascribed to primary size of the SAPO-34 particles [43].

The operando experiment conducted within the Linkam CCR1000 reactor cell points out a similar chemistry with respect to the one performed with the magnetic stirring setup, however occurring with a completely different timescale. The data presented in Figure 4 account for a catalyst which is still fully active, containing a small fraction of deactivating species. The initial formation of condensed aromatic species (PAHs) is clearly observed and their signals intensities increase along the whole TOS here investigated. A slight accumulation of heavy alkenes becomes visible only at late TOS, compatibly with the steady-state conversion observed by MS.

3.3 *Comparison of the setups*

The operando UV-Raman experiments reported in Figure 3 and Figure 4 demonstrate the impact of the choice of the setup on the achieved spectroscopic results. Even if the overall chemistry of the hydrocarbon transformation is consistently similar in both cases, the spatiotemporal advancement of these reactions toward deactivating species is certainly different. With the magnetic stirring reactor cell a rapid transformation of PAHs into heavy alkenes is observed, and the major changes take place along the first 20-30 min, while in the remaining 60-70 min only minor changes occur. In contrast, for the fluidized bed reactor along the same time frame, first the build-up of PAHs is observed, followed by a slow but continuous conversion of the same into heavy alkenes. In order to assess the degree of deactivation obtained in the two cases, in Figure 5 the final TOS spectra (90 min) for both the setups are compared with the spectrum of fully deactivated SAPO-34 unloaded from a conventional testing reactor as reported in ref. [8].

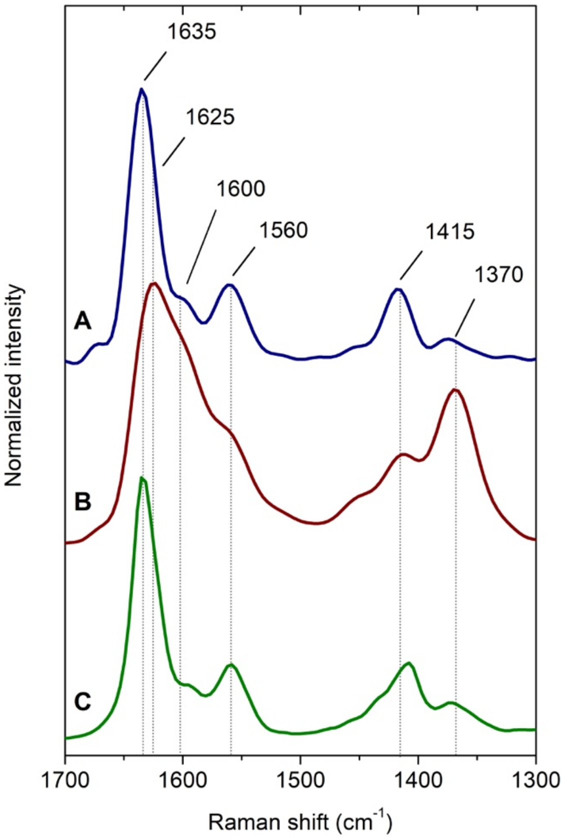

Figure 5. UV-Raman spectra of SAPO-34 collected: A) with the magnetic stirring reactor cell, after 90 min of MTH reaction (400 °C, 2 g_{MeOH} g_{cat}^{-1} h^{-1}); B) with the Linkam CCR1000 reactor cell, after 90 min of MTH reaction (400 °C, 2 g_{MeOH} g_{cat}^{-1} h^{-1}); and C) ex situ on a fully deactivated sample upon 20 h of MTH reaction (400 °C, 2 g_{MeOH} g_{cat}^{-1} h^{-1}) in a conventional testing setup (see ref. [8]).

The final spectrum collected with the magnetic stirring setup closely resembles the one obtained ex situ on a fully deactivated SAPO-34. This observation is thus compatible with a fully deactivated catalyst, which contrasts with the remaining activity observed by MS in the operando experiment. This contradicting behavior can be explained by considering the typical spatiotemporal evolution of the MTH reaction when performed in a fixed bed reactor: the reaction zone and consequently the deactivation occurs first at the top layers and then progressively proceeds toward the bottom of the reactor, in a way often described as a “burning cigar” [18,19,37,38]. Since in the stirring magnet setup the catalyst is loaded as a pellet, it is probed from the top and the sample depth investigated by UV-Raman is limited (below the μm). The obtained result can be rationalized as the observation of the top layers of the fixed bed, whose deactivation occurs much faster in comparison to the whole catalyst pellet/bed.

In the case of the Linkam CCR1000 reactor cell, the molecular features found after 90 min of reaction are instead representative of a fully operating catalyst, in agreement with the low amount of alkenes detected spectroscopically and the steady state conversion followed by the MS. This behavior in the fluidized bed can be explained by a locally lower methanol concentration due to back-mixing with products, leading to a much slower deactivation [39]. As a result, the deactivation occurs homogeneously over the whole catalyst bed, and the laser is probing the Raman signal from fluidized catalyst particles of the integral reactor.

4 Conclusions

In this work, the operando UV-Raman characterization of SAPO-34 during MTH reaction has been presented. In particular, the role of the setup and spatial location of the spectroscopic probe for the study has been discussed. While possible sample damaging induced by the intense excitation source could be avoided in both setups, the presented results have disclosed the importance of the spatial concentration profiles in a reactor and how these can be observed by spectroscopy. Due to the peculiar spatial deactivation profile of the MTH reaction in a fixed bed reactor, the magnetic stirring setup (mimicking a fixed bed reactor) showed spectroscopic evidences of an advanced degree of deactivation, though the catalyst was found still active by online MS. For the fluidized bed setup, even after the same reaction time, the spectroscopic features and the activity measurements both evidenced a catalyst far from deactivation, as a result of using and probing the integral catalyst bed.

As a general remark, this work wants to emphasize the importance of the choice of the setup in determining the measurement outcomes in all the cases where spatiotemporal resolution is critical parameter: a critical discussion of the data on the basis of the adopted technique/setup is compulsory, as exemplified in this report.

Acknowledgments

This work is part of the MS and DRG PhD theses. This publication is part of the European Industrial Doctorate Project “ZeoMorph” (Grant Agreement No. 606965). The financial support from the European Research Council via Marie Curie Actions (FP7- PEOPLE-2013-ITN-EID) is acknowledged. Dr. Anna M. Lind and Dr. Bjørnar Arstad at SINTEF Materials and Chemistry are kindly acknowledged for preparing the SAPO-34 catalyst. MS, FB and SB acknowledge Open Access Labs project for funding (2013-2015 agreement of Compagnia di San Paolo and Università di Torino).

References

[1] S. Kvisle, T. Fuglerud, S. Kolboe, U. Olsbye, K.P. Lillerud, B. V. Vora, Methanol-to-Hydrocarbons, in: Handb. Heterog. Catal., Wiley-VCH Verlag GmbH & Co. KGaA, Weinheim, Germany, 2008: pp. 2950–2965. doi:10.1002/9783527610044.hetcat0149.

[2] C.D. Chang, Hydrocarbons from Methanol, Catal. Rev. 25 (1983) 1–118. doi:10.1080/01614948308078874.

[3] U. Olsbye, S. Svelle, M. Bjørgen, P. Beato, T.V.W. Janssens, F. Joensen, S. Bordiga, K.P. Lillerud, Conversion of Methanol to Hydrocarbons: How Zeolite Cavity and Pore Size Controls Product Selectivity, Angew. Chem. Int. Ed. 51 (2012) 5810–5831. doi:10.1002/anie.201103657.

[4] B. Smit, T.L.M. Maesen, Towards a molecular understanding of shape selectivity., Nature. 451 (2008) 671–678. doi:10.1038/nature06552.

[5] J.W. Park, J.Y. Lee, K.S. Kim, S.B. Hong, G. Seo, Effects of cage shape and size of 8-membered ring molecular sieves on their deactivation in methanol-to-olefin (MTO) reactions, Appl. Catal. A Gen. 339 (2008) 36–44. doi:10.1016/j.apcata.2008.01.005.

[6] H. Schulz, “Coking” of zeolites during methanol conversion: Basic reactions of the MTO-, MTP- and MTG processes, Catal. Today. 154 (2010) 183–194. doi:10.1016/j.cattod.2010.05.012.

[7] M. Guisnet, P. Magnoux, Coking and deactivation of zeolites: influence of the pore structure, Appl. Catal. 54 (1989) 1–27. doi:10.1016/S0166-9834(00)82350-7.

[8] D. Rojo-Gama, M. Signorile, F. Bonino, S. Bordiga, U. Olsbye, K.P. Lillerud, P. Beato, S. Svelle, Structure–deactivation relationships in zeolites during the methanol–to-hydrocarbons reaction:

Complementary assessments of the coke content, J. Catal. 351 (2017) 33–48. doi:10.1016/j.jcat.2017.04.015.

[9] F.L. Bleken, K. Barbera, F. Bonino, U. Olsbye, K.P. Lillerud, S. Bordiga, P. Beato, T.V.W. Janssens, S. Svelle, Catalyst deactivation by coke formation in microporous and desilicated zeolite H-ZSM-5 during the conversion of methanol to hydrocarbons, J. Catal. 307 (2013) 62–73. doi:10.1016/j.jcat.2013.07.004.

[10] P. Beato, E. Schachtl, K. Barbera, F. Bonino, S. Bordiga, Operando Raman spectroscopy applying novel fluidized bed micro-reactor technology, Catal. Today. 205 (2013) 128–133. doi:10.1016/j.cattod.2012.09.030.

[11] Y. Chua, P.C. Stair, A Novel Fluidized Bed Technique for Measuring UV Raman Spectra of Catalysts and Adsorbates, J. Catal. 196 (2000) 66–72. doi:10.1006/jcat.2000.3017.

[12] Y.T. Chua, P.C. Stair, An ultraviolet Raman spectroscopic study of coke formation in methanol to hydrocarbons conversion over zeolite H-MFI, J. Catal. 213 (2003) 39–46. doi:10.1016/s0021-9517(02)00026-x.

[13] C. Li, P.C. Stair, Ultraviolet Raman spectroscopy characterization of coke formation in zeolites, Catal. Today. 33 (1997) 353–360. doi:10.1016/s0920-5861(96)00120-4.

[14] E. Borodina, F. Meirer, I. Lezcano-González, M. Mokhtar, A.M. Asiri, S.A. Al-Thabaiti, S.N. Basahel, J. Ruiz-Martinez, B.M. Weckhuysen, I. Lezcano-González, M. Mokhtar, A.M. Asiri, S.A. Al-Thabaiti, S.N. Basahel, J. Ruiz-Martinez, B.M. Weckhuysen, Influence of the Reaction Temperature on the Nature of the Active and Deactivating Species during Methanol to Olefins Conversion over H-SSZ-13, ACS Catal. 5 (2015) 992–1003. doi:10.1021/cs501345g.

[15] P. Del Campo, W.A. Slawinski, R. Henry, M.W. Erichsen, S. Svelle, P. Beato, D. Wragg, U. Olsbye, Time- and space-resolved high energy operando X-ray diffraction for monitoring the methanol to hydrocarbons reaction over H-ZSM-22 zeolite catalyst in different conditions, Surf. Sci. 648 (2016) 141–149. doi:10.1016/j.susc.2015.10.049.

[16] J. Goetze, F. Meirer, I. Yarulina, J. Gascon, F. Kapteijn, J. Ruiz-Martínez, B.M. Weckhuysen, Insights into the Activity and Deactivation of the Methanol-to-Olefins Process over Different Small-Pore Zeolites As Studied with Operando UV-vis Spectroscopy, ACS Catal. 7 (2017) 4033–4046. doi:10.1021/acscatal.6b03677.

[17] Q. Qian, C. Vogt, M. Mokhtar, A.M. Asiri, S.A. Al-Thabaiti, S.N. Basahel, J. Ruiz-Martínez, B.M. Weckhuysen, Combined operando UV/Vis/IR spectroscopy reveals the role of methoxy and aromatic species during the methanol-to-olefins reaction over H-SAPO-34, ChemCatChem. 6 (2014) 3396–3408. doi:10.1002/cctc.201402714.

[18] D. Rojo-Gama, S. Etemadi, E. Kirby, K.P. Lillerud, P. Beato, S. Svelle, U. Olsbye, Time- and space-resolved study of the methanol to hydrocarbons (MTH) reaction – influence of zeolite topology on axial deactivation patterns, Faraday Discuss. 197 (2017) 421–446. doi:10.1039/C6FD00187D.

[19] D. Rojo-Gama, L. Mentel, G.N. Kalantzopoulos, D.K. Pappas, I. Dovgaliuk, U. Olsbye, K.P. Lillerud, P. Beato, L.F. Lundegaard, D.S. Wragg, S. Svelle, Deactivation of Zeolite Catalyst H-ZSM-5 during Conversion of Methanol to Gasoline: Operando Time- and Space-Resolved X-ray Diffraction, J. Phys. Chem. Lett. 9 (2018) 1324–1328. doi:10.1021/acs.jpclett.8b00094.

[20] D.S. Wragg, M.G. O'Brien, F.L. Bleken, M. Di Michiel, U. Olsbye, H. Fjellvåg, Watching the methanol-to-olefin process with time- and space-resolved high-energy operando X-ray diffraction, Angew. Chem. Int. Ed. 51 (2012) 7956–7959. doi:10.1002/anie.201203462.

[21] H. An, F. Zhang, Z. Guan, X. Liu, F. Fan, C. Li, Investigating the Coke Formation Mechanism of H-ZSM-5 during Methanol Dehydration Using Operando UV-Raman Spectroscopy, ACS Catal. (2018). doi:10.1021/acscatal.8b00928.

[22] a. Ferrari, J. Robertson, Interpretation of Raman spectra of disordered and amorphous carbon, Phys. Rev. B. 61 (2000) 14095–14107. doi:10.1103/PhysRevB.61.14095.

[23] A.C. Ferrari, J. Robertson, Resonant Raman spectroscopy of disordered, amorphous, and diamondlike carbon, Phys. Rev. B. 64 (2001) 075414. doi:10.1103/PhysRevB.64.075414.

[24] S. Shim, C.M. Stuart, R.A. Mathies, Resonance Raman Cross-Sections and Vibronic Analysis of Rhodamine 6G from Broadband Stimulated Raman Spectroscopy, ChemPhysChem. 9 (2008) 697–699. doi:10.1002/cphc.200700856.

[25] E.C. Le Ru, L.C. Schroeter, P.G. Etchegoin, Direct Measurement of Resonance Raman Spectra and Cross Sections by a Polarization Difference Technique, Anal. Chem. 84 (2012) 5074–5079. doi:10.1021/ac300763q.

[26] W.R. Silva, E.L. Keller, R.R. Frontiera, Determination of Resonance Raman Cross-Sections for Use in Biological SERS Sensing with Femtosecond Stimulated Raman Spectroscopy, Anal. Chem. 86 (2014) 7782–7787. doi:10.1021/ac501701h.

[27] J.W. Patterson, The Ultraviolet Absorption Spectra of Coronene, J. Am. Chem. Soc. 64 (1942) 1485–1486. doi:10.1021/ja01258a505.

[28] J. Catalán, J.C. Del Valle, A spectroscopic rule from the solvatochromism of aromatic solutes in nonpolar solvents, J. Phys. Chem. B. 118 (2014) 5168–5176. doi:10.1021/jp501685y.

[29] J. Ferguson, L.W. Reeves, W.G. Schneider, Vapor Absorption Spectra and Oscillator Strengths of Naphthalene, Anthracene, and Pyrene, Can. J. Chem. 35 (1957) 1117–1136. doi:10.1139/v57-152.

[30] W. Kiefer, H.J. Bernstein, Rotating Raman Sample Technique for Colored Crystal Powders; Resonance Raman Effect in Solid KMnO4, Appl. Spectrosc. 25 (1971) 609–613. doi:10.1366/000370271779951101.

[31] C.P. Cheng, J.D. Ludowise, G.L. Schrader, Controlled-Atmosphere Rotating Cell for in Situ Studies of Catalysts Using Laser Raman Spectroscopy, Appl. Spectrosc. 34 (1980) 146–150. doi:10.1366/0003702804730727.

[32] A. Müller, T. Weber, In situ raman investigation of hydrodesulphurization catalysts, Appl. Catal. 77 (1991) 243–250. doi:10.1016/0166-9834(91)80069-9.

[33] A. Damin, M. Signorile, F. Bonino, S. Bordiga, R. Disa, A method for analysis by Raman spectroscopy, WO2017077513 (A1), 2017.

[34] M. Signorile, F. Bonino, A. Damin, S. Bordiga, A novel Raman setup based on magnetic-driven rotation of sample, Top. Catal. (2018). doi:10.1007/s11244-018-1033-z.

[35] M. Signorile, F. Bonino, A. Damin, S. Bordiga, In Situ Resonant UV-Raman Spectroscopy of Polycyclic Aromatic Hydrocarbons, J. Phys. Chem. C. 119 (2015) 11694–11698. doi:10.1021/acs.jpcc.5b02209.

[36] M. Signorile, F. Bonino, A. Damin, S. Bordiga, UV-Raman Fingerprint of Brønsted Sites in MFI Zeolites: A Useful Marker in Dealumination Detection, J. Phys. Chem. C. 120 (2016) 18088–18092. doi:10.1021/acs.jpcc.6b05520.

[37] D. Rojo-Gama, M. Nielsen, D.S. Wragg, M. Dyballa, J. Holzinger, H. Falsig, L.F. Lundegaard, P. Beato, R.Y. Brogaard, K.P. Lillerud, U. Olsbye, S. Svelle, A Straightforward Descriptor for the Deactivation of Zeolite Catalyst H-ZSM-5, ACS Catal. 7 (2017) 8235–8246. doi:10.1021/acscatal.7b02193.

[38] J.F. Haw, D.M. Marcus, Well-defined (supra)molecular structures in zeolite methanol-to-olefin catalysis, Top. Catal. 34 (2005) 41–48. doi:10.1007/s11244-005-3798-0.

[39] S. Müller, Y. Liu, M. Vishnuvarthan, X. Sun, A.C. Van Veen, G.L. Haller, M. Sanchez-Sanchez, J.A. Lercher, Coke formation and deactivation pathways on H-ZSM-5 in the conversion of methanol to olefins, J. Catal. 325 (2015) 48–59. doi:10.1016/j.jcat.2015.02.013.

[40] Framework Type CHA, (2007). http://europe.iza-structure.org/IZA-SC/framework.php?STC=CHA.

[41] N. Sheppard, D.M. Simpson, The infra-red and Raman spectra of hydrocarbons. Part I. Acetylenes and olefins, Q. Rev. Chem. Soc. 6 (1952) 1. doi:10.1039/qr9520600001.

[42] B.P.C. Hereijgers, F. Bleken, M.H. Nilsen, S. Svelle, K.P. Lillerud, M. Bjørgen, B.M. Weckhuysen, U. Olsbye, Product shape selectivity dominates the Methanol-to-Olefins (MTO) reaction over H-SAPO-34 catalysts, J. Catal. 264 (2009) 77–87. doi:10.1016/j.jcat.2009.03.009.

[43] K.Y. Lee, H.J. Chae, S.Y. Jeong, G. Seo, Effect of crystallite size of SAPO-34 catalysts on their induction period and deactivation in methanol-to-olefin reactions, Appl. Catal. A Gen. 369 (2009) 60–66. doi:10.1016/j.apcata.2009.08.033.